J Mater Sci (2008) 43:1948–1957
DOI 10.1007/s10853-007-2406-z

Recombination of silica and zirconia into zircon by means of laser treatment of plasma-sprayed coatings

S. Schelz · F. Enguehard · N. Caron · D. Plessis · B. Minot · F. Guillet · J.-L. Longuet · N. Teneze · E. Bruneton

Received: 4 December 2006 / Accepted: 13 December 2007 / Published online: 30 January 2008

Abstract Self-supported zircon ($ZrSiO_4$) coatings have been deposited by means of atmospheric pressure plasma spraying, a high growth rate deposition method. However, it is well known that $ZrSiO_4$ dissociates into ZrO_2 and SiO_2 in the high-temperature plasma torch during plasma spraying, the rapid quenching preventing reverse combination of both components into $ZrSiO_4$. Usually, high-temperature annealing (1,600–1,900 K) is applied to recombine SiO_2 and ZrO_2 into $ZrSiO_4$. In this contribution, we investigate an attractive technological alternative to recombine SiO_2 and ZrO_2 into $ZrSiO_4$ by laser treatment with a scanning continuous wave CO_2 laser. By carefully adjusting the CO_2 laser treatment parameters (laser power density and scanning velocity), we show that the SiO_2 and ZrO_2 phases indeed recombine into $ZrSiO_4$, however, with a very low recombination rate. Thus, we have investigated the addition of SiO_2-rich glassy particles to the plasma spray powders to facilitate the recombination of ZrO_2, and SiO_2 into $ZrSiO_4$ during the laser treatment. Furthermore, the beneficial role of the glassy particles addition to substantially lower the annealing temperature during classical heat treatments has been studied. Available evidence indicates that the glassy particles melt during heat treatment, and thus favor the mobility and availability of silica at the ZrO_2 grains, which results in a lowering of the reaction temperature and an enhancement of the reaction kinetics.

S. Schelz (✉) · F. Enguehard · N. Caron · D. Plessis · B. Minot · F. Guillet · J.-L. Longuet · N. Teneze · E. Bruneton
CEA/Le Ripault, B. P. 16, 37260 Monts, France
e-mail: sabine.schelz@cea.fr

Introduction

Zircon, $ZrSiO_4$, is highly chemically inert at both low and high temperatures [1]. It shows excellent thermal shock resistance, very low thermal expansion coefficient (5.3×10^{-6} K^{-1} from 300 to 1,773 K), and low thermal conductivity (6.1 W m^{-1} K^{-1} at 373 K and 4.0 W m^{-1} K^{-1} at 1,773 K [2–4]). Its mechanical strength does not alter even at temperatures higher than 1,673 K [5, 6]. Although difficult, the preparation of high-purity $ZrSiO_4$ has already been the subject of a great number of research papers [7–11].

The phase diagram of the SiO_2 and ZrO_2 binary system [12] shows only zircon as an intermediate phase (Fig. 1). Below 1,949 K, crystalline ZrO_2 and amorphous SiO_2 tend to react to form the stable zircon phase [13]. In general, the preparation of zircon by solid-state reaction requires a thermal treatment at 1,673–1,873 K in air [14, 15]. It has been reported that zircon is formed at temperatures as low as 1,473 K, essentially from amorphous silica and tetragonal zirconia (t-ZrO_2) [11]. Formation of zircon predominates over the transformation of amorphous silica to cristobalite in the mixture. Zircon preparation by means of sol–gel synthesis from alkoxide precursors [7, 16] and the hydrothermal synthesis was also investigated. As early as 1957, Frondel and Colette [17] showed that zircon can be obtained from gelatinous zirconia and silica by hydrothermal treatment at 673 K for 168 h at 1,000 bar. Several studies have been carried out by varying the synthesis parameters (temperature, time, pH) [18, 19]. More recently, Valéro et al. [8] have synthesized porous zircon from basic fluorinated synthesis gels at 423 K under autogenous pressure (about 5 bar). Furthermore, Shoyama et al. [20] examined the formation process of zircon in the sol–gel derived $SiO_2 \cdot ZrO_2$ gels added with different kinds of lithium compounds. The addition of lithium ions to the $SiO_2 \cdot ZrO_2$ gels was found to

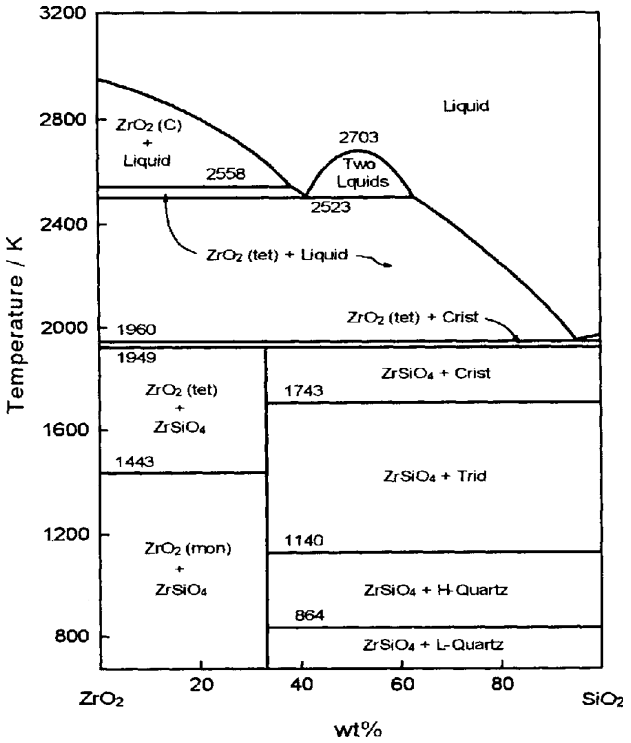

Fig. 1 Phase diagram of ZrO_2–SiO_2

be very effective to produce zircon at temperatures as low as 1,073–1,173 K and ambient pressure.

Plasma spraying is a convenient method to produce large-area coatings with high-growth rates, necessary for many applications [21]. $ZrSiO_4$ is among the cheapest spraying materials for refractory applications. However, $ZrSiO_4$ is thermodynamically unstable above 1,949 K, when it starts dimixing into zirconia and silica. Hence, $ZrSiO_4$ dissociates in a thermal plasma into ZrO_2 and SiO_2, the rapid quenching preventing reverse combination of both components [22, 23]. The large difference between melting points of ZrO_2 and SiO_2 causes first crystalline metastable ZrO_2 to precipitate from the melt and only then the glassy phase of SiO_2 solidifies. The plasma-sprayed $ZrSiO_4$ material consists therefore of pores, glassy-phase SiO_2, and finely dispersed crystalline ZrO_2 [22]. When zircon as a final product is desired, usually high-temperature annealing is applied.

In the past few years, laser surface treatment has proved to be an efficient technique for the surface modification of refractories [24–27]. A zircon refractory was surface melted with a pulsed Nd:YAG laser to introduce AlN nanoparticles with the aim of improving its surface density and modifying its corresponding microstructure [28]. In an earlier study, the same authors also treated a zircon refractory, that time by CO_2 laser surface melting [4]. Laser melting treatment led to the decomposition of $ZrSiO_4$ into ZrO_2 and SiO_2. In the present contribution, laser treatment is expected to produce the opposite, namely to recombine ZrO_2 and SiO_2 present in the plasma-sprayed coatings (since $ZrSiO_4$ dissociates in a plasma into ZrO_2 and SiO_2) into $ZrSiO_4$. For many applications, it might be an advantage to avoid high-temperature annealing up to 1,900 K for several hours. Thus, laser annealing might offer an attractive technological alternative to recombine ZrO_2 and SiO_2 into $ZrSiO_4$. The results of such a treatment are presented in this contribution. It will be shown that the addition of the glassy particles strongly stimulates the combination of SiO_2 and ZrO_2 into $ZrSiO_4$. Furthermore, it is shown that the presence of glassy particles in the coating also results in a lowering of the reaction temperature to recombine ZrO_2 and SiO_2 into $ZrSiO_4$ during classical heat treatments.

Experimental

The materials used in this investigation were commercially available $ZrSiO_4$ powders with a particle size distribution ranging between 22 and 45 μm (Medipure Powder). The commercial powder certificate indicates following impurities: HfO_2 (level not indicated), 0.2 wt% Al_2O_3, <0.1 wt% TiO_2, <0.1 wt% Fe_2O_3, <0.1 wt% CaO, <0.1 wt% MgO. The coatings were deposited by atmospheric plasma spraying [21] using a Sulzer Metco plasma torch. The powder was injected radially downstream from the nozzle exit at a constant feeding rate (20 g/min). The carrier gas flow rate was adjusted in such a way that the mean particle trajectory within the plasma jet was optimized to enhance the particle treatment during its travel within the plasma. However, the main plasma parameters (plasma gas, arc current, spraying distance) were not optimized to obtain a high level of incorporated $ZrSiO_4$ in the final coating.

The addition of SiO_2-rich glassy particles (particle size distribution between 1.5 and 50 μm) to the $ZrSiO_4$ powders has also been investigated. These glassy particles are mainly composed of 36 ± 2 wt% B_2O_3, 31 ± 2 wt% SiO_2, 16.7 ± 0.8 wt% Na_2O, 7.6 ± 0.4 wt% CaO, and 3.6 ± 0.2 wt% MgO, as well as Al_2O_3, ZnO, Fe_2O_3, TiO_2, and K_2O which are below 1 wt%. Their softening temperature is 983 K. The powder mixture was injected through an injector located close to the nozzle exit in the plasma plume.

The as-deposited coatings presented open porosities ranging between 16% and 20% depending on the compositions of the mixtures. For this study, two coatings were fabricated and subsequently submitted to laser treatments: the first coating, approximately 350-μm thick, did not contain any glassy particles at all, whereas the second coating, approximately 300-μm thick, contained 30 wt%

glassy particles. Both coatings were removed from their aluminum substrates and were placed on highly thermally insulating supports made of very porous (porosity $\approx$ 90%) nanostructured materials before the laser and classical heat treatments.

The laser treatments were carried out using a continuous wave CO_2 laser operated in the monomode TEM00 configuration, hence presenting a Gaussian surface profile. The laser beam was focused on the sample surface by means of a ZnSe converging lens with a focal distance of 150 mm. The distance between the lens and the sample surface was varied, leading to different beam sizes and power surface densities. The Gaussian radius (σ) at $1/e$ of the laser irradiation at the sample surface was measured experimentally for each optical configuration. The scanning velocity v was varied between 0.005 and 0.05 mm s^{-1}. The incident laser power P_i at the sample surface was maintained at the value of 8 W. The equivalent power density "entering" the sample (φ_s) has been defined as $(1 - R)\cdot\varphi_i$, where φ_i is the equivalent power density "arriving" at the surface and R the intensity of the hemispherical reflection coefficient before laser treatment. $R = 0.07$ for both kinds of samples (samples containing or not the glassy particles). φ_i, the equivalent power density "arriving" at the surface, is defined as:

$$\varphi_i = P_i/\pi\sigma^2,$$

with P_i: incident laser power on the sample (8 W) and σ the Gaussian beam radius at $1/e$.

Thus the equivalent power density "entering" the sample is

$$\varphi_s = (1 - R)P_i/\pi\sigma^2.$$

Three different laser treatment experiments, corresponding to three different values of the couple (σ, v), were performed on the coating without glassy particles' and one laser treatment experiment was performed on the coating containing glassy particles. The laser process parameters (σ, v) of these four experiments are summarized in Table 1.

Table 1 Laser process parameters, such as Gaussian beam radius (σ), lateral distance (s) between scanning lines, power density "entering" the sample (φ_s), and scanning velocity (v), as well as the concentration of glassy particles in the sample

Treatment no.	Glassy particles (wt%)	σ (mm)	s (mm)	φ_s (W cm^{-2})	v (mm s^{-1})
1	0	1.5	0.5	105.2	0.05
2	0	1.5	0.5	105.2	0.005
4	0	2	0.75	59.2	0.01
9	30	2	0.75	59.2	0.01

Some of the plasma-sprayed coatings have been air-annealed in a furnace at different temperatures: 1,173, 1,373, 1,573, and 1,773 K to compare the efficiency of our laser treatment to the one of a conventional heat treatment in terms of recombination of ZrO_2 and SiO_2 into $ZrSiO_4$ and also to investigate the efficiency of glassy particles' addition on the lowering of the recombination temperature.

The film structures were studied using X-ray diffraction (XRD) on a BRUKER D5000 diffractometer equipped with a copper anode (Cu $K\alpha_{1,2}$). The coatings were hand milled prior to analysis. It may be shown by very simple heat conduction arguments that the temperature within the coating thickness is quite homogeneous; therefore, the XRD spectra of the milled coatings are representative for the surface as well as for the back side crystalline structures. Phase indexing requires the removal of background signal; hence, the XRD diagrams shown in this work do not account for small amounts of vitreous phases as glassy SiO_2.

The morphology of the samples has been observed before and after laser treatments by optical microscopy. For this purpose, the samples have been embedded in a resin and polished on their cross-section side.

Film microchemistry was studied by Electron Probe MicroAnalysis (EPMA) on a CAMECA SX50 equipped with four wavelength dispersive spectrometers (WDS). The samples have been prepared with an epoxy resin, polished on their cross-section side, and carbon coated prior to analysis. To visualize the distribution of the glassy particles before and after heat treatment at 1,573 K, X-ray maps of various elements (Zr, Si, O, B, Na, Ca, Mg, C) were recorded over a square approximately 500 μm in size with 2 μm resolution.

Results and discussion

Figure 2 shows the XRD diagrams of five samples sprayed in identical conditions (without adding glassy particles to the $ZrSiO_4$ powder), but with different treatments after deposition. The bottom curve presents the XRD profile of the as-deposited sample. The next two curves from the bottom present the XRD diagrams of laser-treated samples with a laser power density of 105 W cm^{-2} and different scanning velocities (treatment 1: scanning velocity of 0.05 mm s^{-1}; treatment 2: scanning velocity of 0.005 mm s^{-1}). For comparison, the two upper curves of Fig. 1 present the XRD diagrams of samples which have been annealed at 1,773 K in a furnace for 6 and 12 h, respectively. The bottom curve of Fig. 1 reveals the presence of tetragonal ZrO_2 peaks; however, no $ZrSiO_4$ is observable. This is in agreement with earlier studies on plasma-sprayed $ZrSiO_4$ [22], where dimixion of $ZrSiO_4$

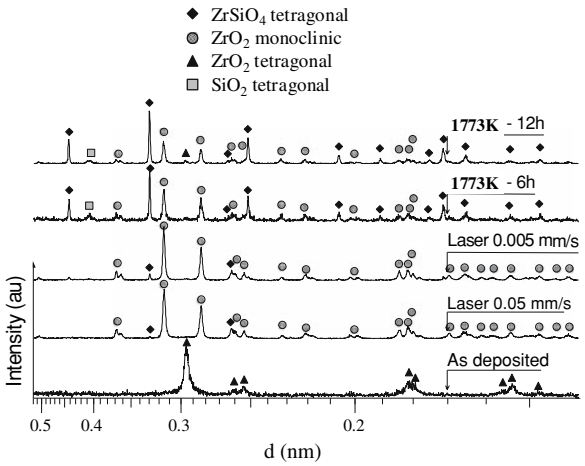

Fig. 2 XRD diagrams of the sample without addition of glassy particles. Bottom curve: as-deposited; next two curves from the bottom: after laser treatment (power density of 105 W cm^{-2}, scanning velocity of 0.05 mm s^{-1} (treatment 1) and 0.005 mm s^{-1} (treatment 2), respectively; top curves: after heat treatment in a furnace at 1,773 K during 6 h and 12 h, respectively

into SiO_2 and ZrO_2 has been observed during plasma spraying. Whether the crystalline ZrO_2 will be cubic, tetragonal, or monoclinic depends on the quenching rate [22]. After laser treatment with a power density of 105 W cm^{-2} and a scanning velocity of 0.05 mm s^{-1}, the tetragonal ZrO_2 transformed to the monoclinic ZrO_2 phase; traces of zircon are also observed. When decreasing the scanning velocity (0.005 mm s^{-1}), the zircon peak slightly increases, indicating a beginning of recombination of ZrO_2 and SiO_2 into $ZrSiO_4$. For comparison purposes, the heat treatment at 1,773 K for 6 and 12 h yielded a much larger amount of zircon. However the monoclinic ZrO_2 phase is still present, as well as a cristobalite tetragonal SiO_2 phase.

It has already been shown that a total retransformation to zircon can be achieved using a high-temperature treatment (usually between 1,600 and 1,900 K) by the following solid-solid reaction between the crystalline zirconia (c-ZrO_2) and the amorphous silica (a-SiO_2) [29]:

$$\text{a-SiO}_2 + \text{c-ZrO}_2 \rightarrow \text{ZrSiO}_4. \quad (1)$$

The authors have also shown that the limiting phenomenon for zircon formation is the diffusion of silicon through a zircon layer, from an external either continuous or granular silica phase to the surface of the zirconia grains. They evaluated an apparent coefficient for this diffusion (10.6×10^{-18} m^2 s^{-1} at 1,673 K). This very low value is consistent with the very low reaction kinetics observed with our plasma-sprayed coatings. The formation kinetics of the zircon phase has been represented by Weng-Cheng J. Wei and R. Adams in a transformation-temperature-time diagram [30]. This diagram shows transformation curves with a maximum reaction rate near 1,873 K. It typically takes several hours to form the zircon phase with a 50–70% transformation rate at heat temperatures between 1,723 and 1,923 K. This is in quite good agreement with our observed reaction rates during conventional heat treatment in a furnace.

As seen in Fig. 2, the laser treatment employed in this study does not produce substantial amount of recombined $ZrSiO_4$. We have estimated the temperature reached within the coating during laser exposure with the help of a simplified heat transfer model, taking into account radial thermal conduction, heat deposition from the laser beam, and radiative heat exchanges with the environment. The estimated temperatures are between approximately 1,400 and 1,900 K, depending on different model assumptions and laser parameters. These temperatures are consistent with the temperatures during which reaction (1) generally occurs. However, the duration during which a point of the surface is exposed to the laser beam is approximately only 1 min; hence, such low $ZrSiO_4$ concentrations might be expected. Decreasing the scanning velocity—and hence increasing the laser treatment duration—actually increased the $ZrSiO_4$ phase concentration within the coating (treatments 1 and 2). As deduced from the simplified thermal model, the temperature in the coating is in both laser treatment cases approximately the same; however, when decreasing the scanning velocity from 0.05 to 0.005 mm s^{-1}, the treatment time is increased by a factor of 10, which might explain the increase in the zircon concentration.

Increasing the temperature level reached during the laser treatment by increasing the laser power density might possibly increase the $ZrSiO_4$ concentration. However, Wang et al. have shown [4] that high laser energies lead to the dissociation of zircon, much like during plasma spraying. Their CO_2 laser power density was approximately 8 kW cm^{-2}, compared to our 0.1 kW cm^{-2}.

With the aim to enhance reaction kinetics, we have investigated the benefit of a laser treatment combined with additives in the coating. We have studied whether the addition of glassy particles—mainly composed of SiO_2, B_2O_3, and Na_2O—to the plasma spray powder increases the reaction rate of zirconia and silica into $ZrSiO_4$ during the laser treatment. To this end, another sample has been deposited with glassy particles added to the plasma spray powders. The two samples have then been laser treated (treatments 4 and 9) with identical laser parameters (power density of 59 W cm^{-2}, laser scanning velocity of 0.01 mm s^{-1}). Once again, only traces of zircon are detected in the sample without glassy particles' addition, as observed in Fig. 3. The XRD profile of the sample containing 30 wt% glassy particles after laser treatment 9 is compared to the sample without glassy particles after laser treatment 4 (bottom curve: without glassy particles' top curve: 30 wt% glassy particles). This comparison shows

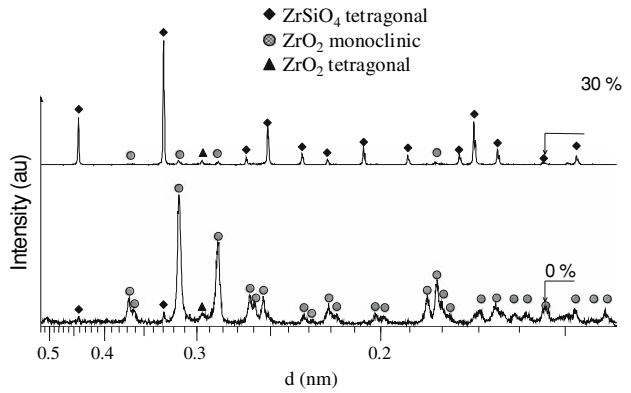

Fig. 3 XRD diagrams of two laser-treated samples (power density of 59 W cm^{-2}, scanning velocity of 0.01 mm s^{-1}). Bottom curve: sample without addition of glassy particles (treatment 4); top curve: sample with addition of 30 wt% glassy particles (treatment 9)

that the addition of the silica-rich glassy particles strongly stimulates the reaction of zirconia and silica into zircon. The diagram recorded on the sample containing glassy particles shows clear intense zircon peaks, whereas the sample without glassy particles and laser treated in the same conditions only reveals a very low amount of zircon.

Figure 4 depicts the XRD diagrams of three glassy particles' (30%) containing samples: an as-deposited sample (bottom curve), a laser-treated sample (treatment 9, middle curve), and a sample annealed during 6 h at 1,773 K in a furnace (top curve). The XRD diagram of the as-deposited sample is very similar to the one of an untreated sample without addition of glassy particles (bottom curve of Fig. 1). The coating contains tetragonal ZrO_2 and amorphous SiO_2 (not observable in the XRD diagram due to background removal). The diagram of the

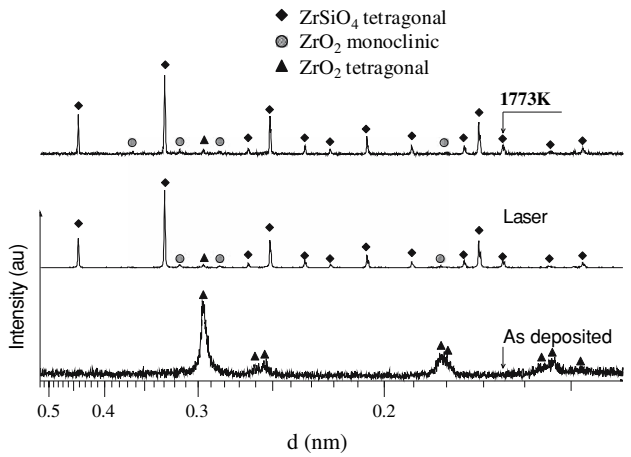

Fig. 4 XRD diagrams of the sample with addition of glassy particles (30 wt%). Bottom curve: as-deposited; middle curve: after laser treatment (power density of 59 W cm^{-2}, scanning velocity of 0.01 mm s^{-1}, treatment 9); top curve: after heat treatment in a furnace during 6 h at 1,773 K

laser-treated sample exhibits very intense zircon peaks. Finally, the XRD diagram of the sample containing 30% glassy particles and annealed at 1,773 K for 6 h is very similar to the one of the laser treated sample, indicating that the laser treatment is as efficient as a heat treatment at 1,773 K during 6 h for glassy particle containing samples.

To get an insight into the coating morphology, the cross-sections of the samples before and after the laser treatments 4 and 9 have been observed by optical microscopy (Figs. 5 and 6, respectively). Before laser treatment, the sample (without glassy particles) exhibits a homogeneous distribution of pores and a lamellar microstructure in which partially melted particles or unmelted ones are embedded. After laser treatment 4, the morphology of this sample is hardly modified. The morphology of the glassy particles containing sample is quite different: the lamellar microstructure is hard to distinguish, while the glassy particles appear as gray flattened spots on the top image (before laser treatment) of Fig. 6. The size and the concentration of these spots correspond to the size and the concentration of the added particles' while their flat shape is attributed to the flattening effect when the glassy particles impinge the substrate surface, commonly observed in plasma-sprayed coatings. The morphology of this sample is strongly modified after laser treatment 9: spots with a large size distribution are now observed with an irregular shape from small branch-like features to very large zones up to 200 μm

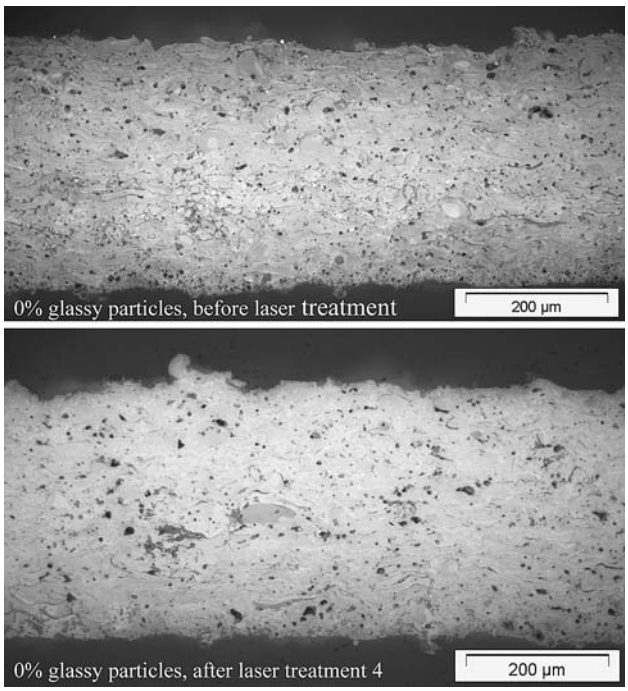

Fig. 5 The cross-section observed by optical microscopy of the sample without glassy particles before and after laser treatment (treatment 4). The sample has been embedded in a resin and polished on their cross-section side before observation

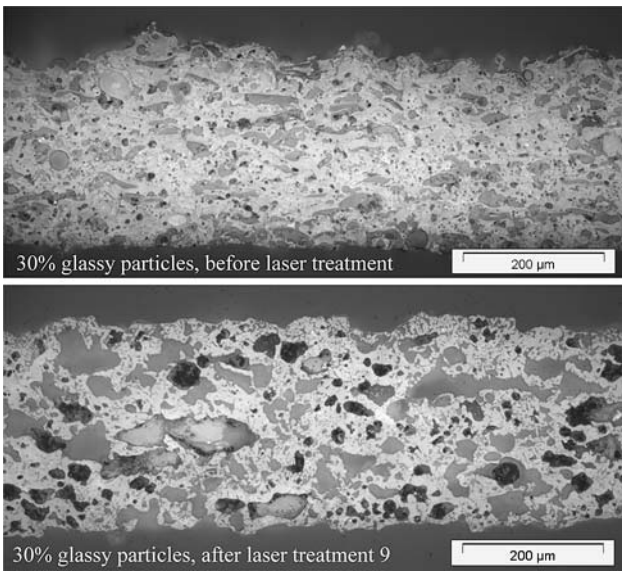

Fig. 6 The cross-section observed by optical microscopy of the sample containing 30% of glassy particles before and after laser treatment (treatment 9). The sample has been embedded in a resin and polished on their cross-section side before observation

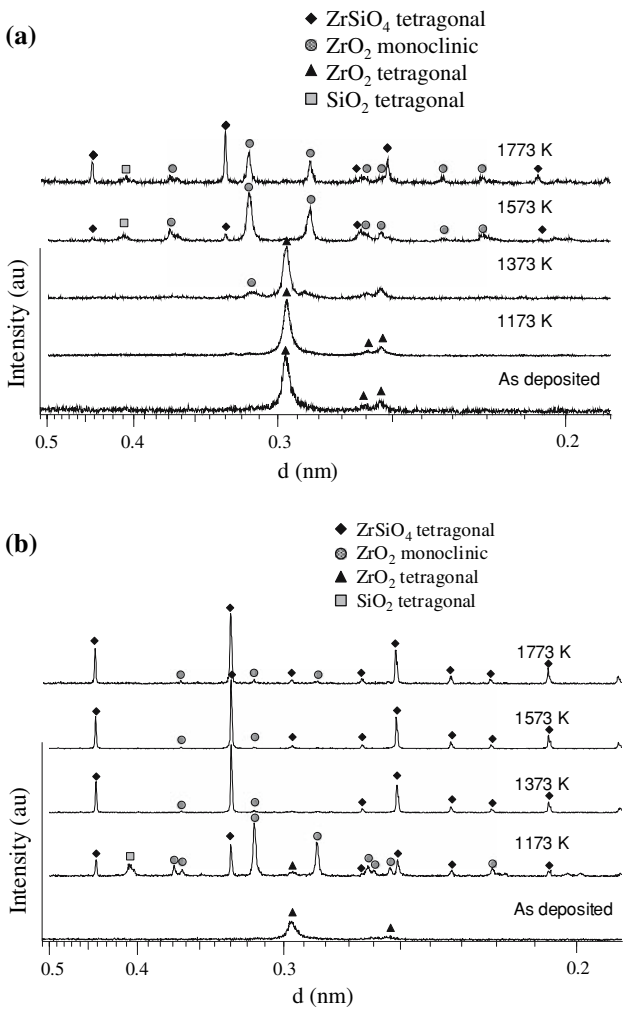

Fig. 7 (**a**) XRD diagrams of the sample without addition of glassy particles before and after annealing at various temperatures during 6 h. (**b**) XRD diagrams of the sample containing 30 wt% of glassy particles before and after annealing at various temperatures during 6 h

in size. As will be shown below by EPMA, a treated sample containing glassy particles is predominantly composed of Zr, O, Si, and a small amount of Mg and Ca.

We also investigated the role of these particles during conventional heat treatments in air. Figure 7a shows the XRD diagrams of a plasma-sprayed $ZrSiO_4$ sample without adding glassy particles to the $ZrSiO_4$ powder and with different heat treatments after deposition. The bottom curve presents the XRD profile of the as-deposited sample. Then, the upper curves of Fig. 7 present XRD diagrams of samples which have been annealed at 1,173, 1,373, 1,573, and 1,773 K in a furnace for 6 h, respectively. The bottom curve (as-deposited sample) and the top curve (annealed at 1,773 K during 6 h) are identical to the ones of Fig. 2. They have been added to Fig. 7a for comparison. After 1,173 and 1,373 K annealing, the XRD diagram only shows tetragonal ZrO_2 peaks like the diagram of the as-deposited sample. After annealing the sample at 1,573 K, zircon peaks of very low intensity appear, indicating a beginning of recombination of ZrO_2 and SiO_2 into $ZrSiO_4$. Finally, the heat treatment at 1,773 K yielded a much larger amount of zircon.

The sample containing 30% glassy particles has also been annealed at different temperatures during 6 h in identical conditions as the sample of Fig. 7a. The XRD profiles before and after heat treatment are shown in Fig. 7b. The XRD diagrams of the as-deposited sample and the one annealed at 1,773 K are identical to those of Fig. 4. They have again been added for comparison purpose. After annealing at 1,173 K the 30% glassy particles containing sample reveals already $ZrSiO_4$ peaks. For comparison, no $ZrSiO_4$ peaks have been detected in the sample without glassy particles' addition after the same heat treatment at 1,173 K. Then after 1,373, 1,573, and 1,773 K annealing a high amount of zirconia and silica has reacted into zircon. By comparing the two samples (without glassy particles and the sample with 30% glassy particles' addition), it becomes again obvious that the addition of the glassy particles strongly enhances the reaction of zirconia and silica into zircon, as already observed after laser treatment. Furthermore, it is clearly shown that the reaction becomes possible at lower annealing temperatures.

Electron probe microanalysis investigations have been carried out on a sample containing 30% glassy particles to visualize more in detail the distribution of the glassy particles before and after heat treatment at 1,573 K. The X-ray maps of various elements (Zr, Si, O, B, Na, Ca, Mg, C)

were recorded over a square approximately 500 μm^2 in size with 2-μm resolution, before (Fig. 8) and after (Fig. 9) annealing at 1,573 K. In Fig. 8, the zirconium X-ray map of the as-deposited sample containing 30% glassy particles shows green and red spots indicating the presence of this element. The dark spots may either be attributed to porosities or zones containing glassy particles (since they do not contain Zr). The porosity of this coating may be visualized by the red spots of the carbon X-ray map, since the carbon originates from the epoxy resin which has penetrated into the sample during preparation. The location of glassy particles in the sample is visualized in the B, Na, Ca, and Mg maps, since these elements originate predominantly from the glassy particles. As seen in the top left corner of the O, B, Na, Ca, and Mg maps, there is an approximately 100-μm large zone which may be attributed to a glassy particle embedded in the coating. In addition, on the Si, Mg, and Ca maps, some further spots are observable having a higher concentration of these elements (red spots) and a lower concentration of B and Na than the large glassy particles zone identified on the left top corner. This indicates that two types of glasses are incorporated in the coating, which might be attributed to a partial decomposition of the glassy particles in the plasma torch. Silicon and oxygen are present both in the glassy particles and in the SiO_2–ZrO_2 matrix. Silicon is distributed quite homogeneously in the whole coating except the porosities, while the concentration of oxygen is higher in the glassy particles than in the SiO_2–ZrO_2 matrix. The size distribution of the glassy particles embedded into the plasma-sprayed coating is quite large, from approximately 10 μm to more than 100 μm in size. Most of them appear as flattened spots on the O, B, Na, Ca, or Mg maps.

After annealing at 1,573 K of the sample (containing 30% glassy particles) (Fig. 9), the Zr, Si, and O X-ray maps indicate that these elements are distributed much more homogeneously in the coating than before annealing, probably corresponding to the $ZrSiO_4$ matrix. This is in agreement with the XRD measurements, where a high amount of $ZrSiO_4$ is observed after annealing of the sample. Dark spots, with a large size distribution from few microns to more than hundred microns, may be attributed to porosity, since there is no evidence of any of the measured elements at these locations. It is quite surprising, that no sodium has been detected after annealing and only small traces of boron. Ca and Mg, originating from the glassy

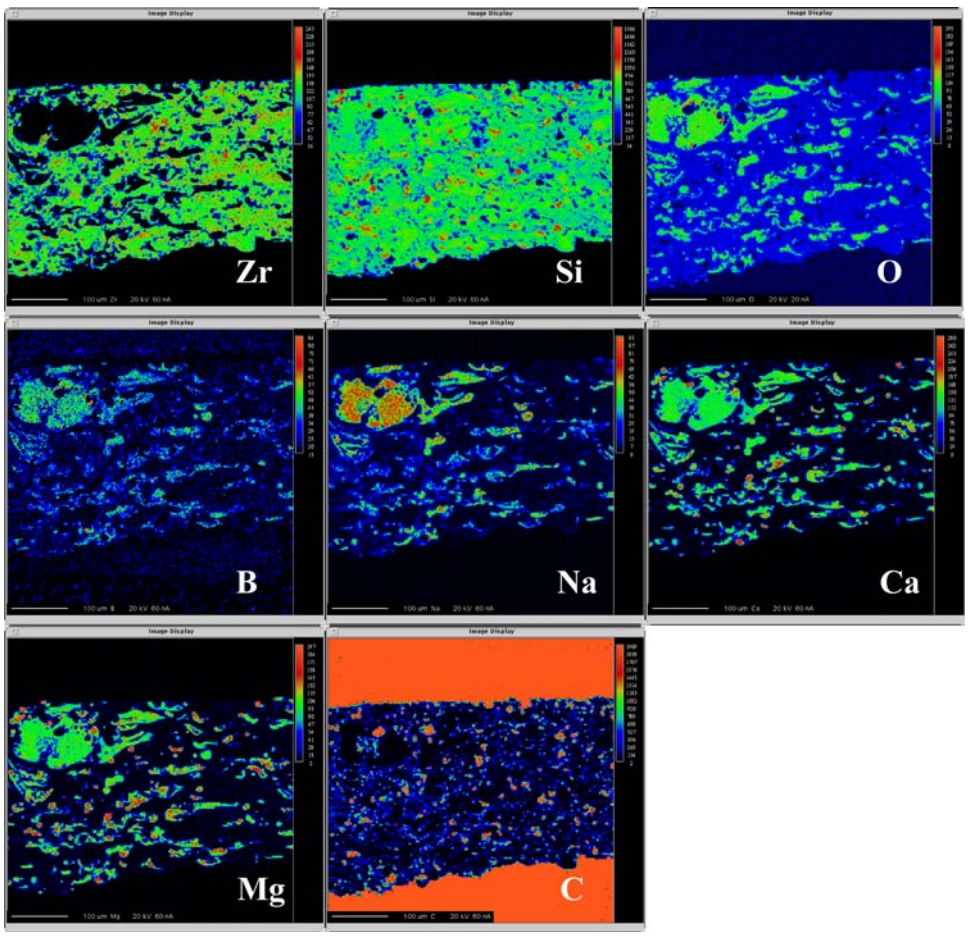

Fig. 8 Electron probe microanalysis X-ray maps of various elements (Zr, Si, O, B, Na, Ca, Mg, C) recorded on the as-deposited sample containing 30% glassy particles before annealing

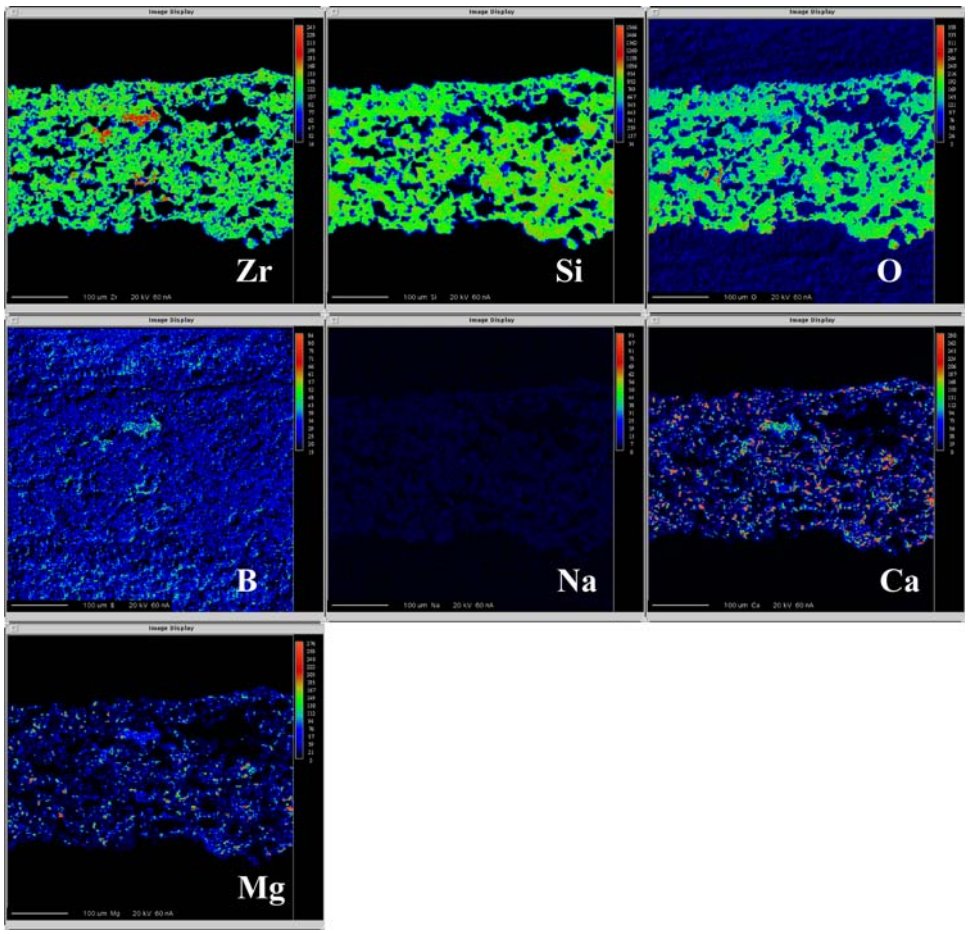

Fig. 9 Electron probe microanalysis X-ray maps of various elements (Zr, Si, O, B, Na, Ca, Mg) recorded on the sample containing 30% glassy particles after annealing at 1,572 K

particles' are now more homogeneously distributed in the coating than before annealing.

Besides SiO_2 and B_2O_3, the glassy particles also contain alkali and earth alkali compounds (Na_2O, CaO, MgO), which might play a role in lowering the reaction temperature. Shoyama et al. [20] have found that the addition of lithium compounds to $ZrO_2 \cdot SiO_2$ gels was very effective to produce zircon at low temperatures. They have discussed several plausible mechanisms for the mineralizing effect of additives on the zircon formation:

1. The addition from liquid phase in the voids between loosely contacted SiO_2 and ZrO_2 particles' through which Zr^{4+} and Si^{4+} ions counterdiffuse to form zircon more easily.
2. Among additives, lithium compounds react with SiO_2 to produce $Li_2Si_2O_5$, with which ZrO_2 reacts to form zircon. $Li_2Si_2O_5$ might be an important intermediate compound to synthesize zircon.
3. Shoyama et al. [20] have found a metastable compound just before the precipitation of zircon and have assigned it to Li_4SiO_4. They interpreted their results by a substitution of Li^+ for Zr^{4+} ions to form $ZrSiO_4$.

In our case, the role of lithium might be replaced by a similar role of Na. For example, an important intermediate compound could be Na_2SiO_3, since the following reaction scheme

$$Na_2SiO_3(l) + ZrO_2(s) \rightarrow ZrSiO_4 + Na_2O(l)$$

has already been proposed by Balek and Trojan [31] at temperatures above 1,173 K. However, as seen below, we tend to attribute the observed reaction boost to mechanism 1.

As observed in the microprobe analysis X-ray maps (Figs. 8 and 9), the microstructure of the coating has completely changed after annealing at 1,573 K. Furthermore, the comparison of the Ca and Mg maps before and after annealing shows that Ca and Mg are distributed more homogeneously in the sample after heat treatment at 1,573 K. This is attributed to diffusion of these elements all over the sample during annealing. Two different concentration levels of Ca and Mg are observable in Fig. 9, which may be attributed to microprecipitates rich in these elements (red spots in the Ca and Mg maps of Fig. 9) and most probably to traces of these elements incorporated in the $ZrSiO_4$ network (blue zones in the Ca and Mg maps of

Fig. 9). However, Na and B are no longer or hardly detectable after the heat treatment. The melting point of Na_2O (melting point of 1,193 K, followed by decomposition) [32] and B_2O_3 (melting point of 723 K and boiling point of 1,523 K) [32] are lower than the applied heat treatments at 1,173–1,773 K. Hence, these oxides have melted and then decomposed and evaporated during annealing of the sample. Some of the liquid phase might also have penetrated into a very porous substrate holder during annealing.

The Ca and Mg elements allow us to trace the glassy particles distribution during annealing. The more homogeneous distribution of Ca and Mg within the coating after annealing might again indicate that the liquid phase, which contains these elements (since they are embedded in the glassy particles') has penetrated into the voids between loosely contacted SiO_2 and ZrO_2 particles. As observed after laser exposure, a treatment duration of only 1 min or so is sufficient to complete the reaction between SiO_2 and ZrO_2 into $ZrSiO_4$. Such a fast formation of $ZrSiO_4$ can be explained by an enhanced diffusion due to the occurrence of the liquid phase, as compared to the characteristic time of a solid-state reaction. Thus, we tend to interpret the observed lowering of the reaction temperature when adding glassy particles by the presence of a liquid phase through which Zr^{4+} and Si^{4+} ions may counterdiffuse to form zircon more easily.

Conclusions

When depositing a zircon coating by means of atmospheric pressure plasma spraying, $ZrSiO_4$ dissociates in the plasma plume into ZrO_2 and SiO_2. We have shown that, by low-energy CO_2 laser treatment, the inverse reaction occurs. However, the zircon concentration is very low (as analyzed by XRD). We have demonstrated that adding low softening point glassy particles (mainly containing B_2O_3, SiO_2, and Na_2O) within the coating results in a strongly enhanced recombination into $ZrSiO_4$. We have also demonstrated that the presence of these glassy particles in the coating results in a lowering of the reaction temperature to recombine SiO_2 and ZrO_2 into $ZrSiO_4$.

The EPMA of the as-deposited sample reveals that the glassy particles are incorporated in the coating with a large-size distribution from approximately 10 μm to more than 100 μm. After annealing, the morphology of the coating has completely changed. Some of the elements, such as Ca and Mg, are distributed more homogeneously within the coating, indicating that these elements have been transported all over the sample and have been partially incorporated in the $ZrSiO_4$ network. However, Na and B are no longer or hardly detectable after the heat treatment; they have probably decomposed and evaporated during annealing of the sample. The lowering of annealing temperature to recombine silica and zirconia into zircon by adding glassy particles has been interpreted in the following way: due to the low softening point of the glassy particles' they melt during annealing and thus penetrate into the voids between loosely contacted SiO_2 and ZrO_2 particles. Thus, Zr^{4+} and Si^{4+} ions may then counterdiffuse in the liquid phase to form zircon more easily.

In conclusion, we have shown that:

(1) the reaction of silica and zirconia into $ZrSiO_4$ during laser treatment can be altered by the activity of added glassy particles into the coating. The adjunction of glassy particles results in a production of a substantial amount of recombined $ZrSiO_4$ with the laser parameters used. Thus, the laser treatment with additives may provide technological benefits over other heat treatment techniques.
(2) the presence of these glassy particles in the coating also results in a lowering of reaction temperatures to recombine SiO_2 and ZrO_2 into $ZrSiO_4$ during classical heat treatments.

Acknowledgements We gratefully acknowledge the technical assistance of Jérôme Lhostis, Charles Froger and Anne-Marie Le Creurer-Hérail. The authors also thank Sébastien Lambert for fruitful discussions and helpful comments.

References

1. Del Pin G, Maschio S, Brückner S, Bachiorrini A (2004) Ceram Int 30:279
2. Orange G, Fantozzi G, Cambier F, Leblud C, Anseau MR, Leriche A (1985) J Mater Sci 20:2533
3. Shackelford JF, Alexander W, Park JS (1994) CRC materials science and engineering handbook. CRC Press, Boca Raton, FL
4. Wang AH, Wang WY, Xie CS, Song WL, Zeng DW (2004) Appl Surf Sci 227:104
5. Mori T (1990) J Ceram Soc Jpn 98(9):1017
6. Shi Y, Huang XX, Yan DS (1994) J Eur Ceram Soc 13(2):113
7. Mori T, Yamamura H, Kobayashi H, Mitamura T (1992) J Am Ceram Soc 75:2420
8. Valéro R, Durand B, Guth J-L, Chopin T (1999) Microporous Mesoporous Mater 29:311
9. Shi Y, Huang X, Yan D (1994) J Eur Ceram Soc 13(2):113
10. Tartaj P, Sanz J, Serna J, Ocana M (1994) J Mater Sci 29:6533
11. Itoh T (1992) J Cryst Growth 125:223
12. Butterman WC, Foster WR (1967) Am Miner 52:880
13. Evans AM, Williamson JPH (1977) J Mater Sci 12:779
14. Curtis CE, Sowman HG (1953) J Am Ceram Soc 36:190
15. Ballaman AA, Laudise RA (1965) J Am Ceram Soc 48:130
16. Kanno Y (1989) J Mater Sci 24:2415
17. Frondel C, Colette RL (1957) Am Miner 42:759
18. Kido H, Komarneni S (1990) Trans Mater Res Soc 1:358
19. Caruba R, Baumer A (1985) Am Miner 70:1224
20. Shoyama M, Matsumoto N, Hashimoto T, Nasu H, Kamiya K (1998) J Mater Sci 33:4821

21. Fauchais P, Vardelle A, Dussoubs B (2001) J Therm Spray Technol 10(1):44
22. Rudajevová A (1994) Surf Coat Technol 64:47
23. Wang E, Wang D (1992) Proceedings of the International Ceramics Conference, Melbourne, p 359
24. Lawrence J, Li L, Spencer JT (1999) Appl Surf Sci 138–139:388
25. Bradley L, Li L, Stott FH (2000) Mater Sci Eng A 278:204
26. Bradley L, Li L, Stott FH (1999) Appl Surf Sci 138–139:233
27. Triantafyllidis D, Li L, Stott FH (2005) Mater Sci Eng A 390:271
28. Wang WY, Wang AH, Zeng DW, Bai ZK, Xie CS, Song WL, Zhu XC (2006) Mater Charact 56:227
29. Veytizou C, Quinson JF, Valfort O, Thomas G (2001) Solid State Ionics 139:315
30. Wei Weng-Cheng J, Adams R (1992) J Eur Ceram Soc 10:291
31. Balek V, Trojan M (1989) Thermochim Acta 143:101
32. Samsonov GV (ed) (1973) The oxide handbook. IFI/Plenum